Triplet Line Shape Simulation in Continuous Wave Electron Paramagnetic Resonance Experiments

AHARON BLANK, HAIM LEVANON

Department of Physical Chemistry and the Farkas Center for Light-Induced Processes, The Hebrew University of Jerusalem, Jerusalem 91904, Israel

ABSTRACT: We present a simple yet powerful method of simulating continuous wave electron spin resonance line shape of triplets in frozen and liquid solutions. The analysis enables one to consider cases such as immobilized triplets with random distribution, anisotropic slow and fast rotation of the triplet molecules, exchange between triplets with different Hamiltonians, anisotropic relaxation rates, and triplets with non-Boltzmann population distribution of the spin levels. Theoretical basis for the method is provided, along with several examples of simulated and experimental spectra for various physical conditions. A short "Matlab" routine, which can be used in the numerical spectra simulation, is given in the Appendix. © 2005 Wiley Periodicals, Inc. Concepts Magn Reson Part A 25A: 18–39, 2005

KEY WORDS: EPR; ESR; triplet; line shape

INTRODUCTION

Electron paramagnetic resonance (EPR) experiments mainly involve systems where the signal originates from a single unpaired electron with two possible

energy levels, referred to as the doublet state. In many important cases, however, stable and photoexcited paramagnetic molecules are found in the triplet state, having three possible energy levels for their two unpaired spins. Examples for such systems are (*1*): O_2 molecule in gas phase; point defects in crystals; transition group and rare earth ions embedded in organic molecules (e.g., V^{3+}, Ni^{2+}); organic aromatic systems (e.g., cyclopentadienylidene), and photoexcited transient triplets (*2*).

The most important information, obtained directly by the EPR experiment, is the EPR spectrum. For the case of triplets, one usually refers to this spectrum as
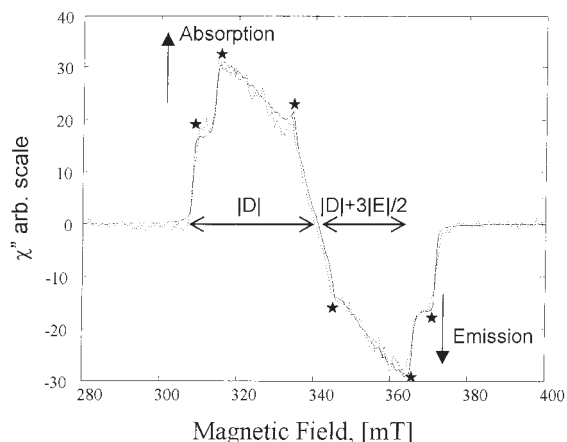
Figure 1 Simulated (solid line) and measured (dashed line) EPR line shape for Ga(tpfc) triplet in frozen toluene at 140 K (borrowed with permission from (3)). Positive sign corresponds to absorption signal; negative sign corresponds to emission signal. The "canonical orientations" are marked with stars. The line shape simulation described in this article found that the best fitting parameters are $A_x = 0.64$; $A_y = 0.47$; $A_z = 0$; $D = -31.6$ mT; $E = 6.73$ mT; $1/T_{2x} = 0.46$ mT; $1/T_{2y} = 0.42$ mT; and $1/T_{2z} = 0.26$ mT.

the EPR line shape, as it often appears as a single inhomogeneously broad line. A typical EPR line shape of randomly oriented photoexcited triplets is shown in Fig. 1. It shows experimental results obtained by time-resolved continuous wave (CW) EPR (3) and their theoretical fit through the line shape simulation that will be described in this article. The time-resolved method acquires the spectrum at a specific time after triplet initiation (usually by a laser pulse). With this method the spectrum is recorded and plotted in its "native" form and not as first derivative, commonly found in doublet state CW EPR (4). The inhomogeneous broadening of the spectrum in Fig. 1 is due to the angular dependence of the spin Hamiltonian, which results in many possible energy levels for such randomly oriented ensemble of triplets. As a consequence of this random orientation, the line shape typically exhibits six pronounced points (marked with stars in Fig. 1), which correspond to the "canonical orientations," at which the magnetic field is oriented along one of the principle axis of the triplet (1). By identifying the points of the canonical orientations on the line shape, one can estimate at first glace, even without elaborate simulations, the triplet's zero field splitting (ZFS) parameters D, E (up to an absolute value), which describe the relative orientation and the distance between the two unpaired spins constituting the triplet (1). Furthermore, the general pattern of the line shape in Fig. 1 (i.e., absorption in low field and

emission in high field) immediately implies that the three triplet levels are polarized (i.e., with non-Boltzmann population distribution of the spin levels) (5, 6). However, the exact nature of this polarization can be revealed only through detailed line shape simulation, which provides the relative population rates to the triplet's X, Y, and Z levels (A_x, A_y, A_z), as described below. Other important parameters, such as the spin-spin relaxation time, T_2, which affects the "sharpness" of the spectrum, and the molecule rotational correlation time, which affects the general line shape pattern, can also be obtained through such line shape simulation.

The triplet line shape simulation is therefore a powerful tool for the extraction of many structural and dynamic molecular parameters. This methodology was employed in the past in many cases. For example, Norris and Weissman used line shape simulation to extract information about rotational diffusion in ground state triplets (7); de Groot and van der Waals investigated conformational interconversions and their effect on the line shape in photoexcited triplets (8); Bramwell and Gendell examined pseudorotation in triplets, through line shape changes (9); and Haarer and Wolf looked at intermolecular energy exchange (10). These early examples set the path for modern research in this field, which attempts to reveal as much information as possible from the EPR line shape. Though some of the research mentioned above is related to stable ground state triplets, most of the modern work in EPR spectroscopy of triplets involves transient species, such as the one described in Fig. 1. Transient triplet species play important role in many photochemical reactions (11). EPR is a unique tool to monitor such intermediates both in terms of its fine time resolution and the high sensitivity of the line shape to dynamic processes.

This article discusses the theoretical approaches that can be employed to analyze quantitatively the triplet line shape of stable and transient species, under various conditions, and to extract the relevant parameters of interest from it. Two main approaches are discussed: the "rotational diffusion" method (12, 13) and the "multiple exchange/discrete jump" method (14, 15). The first method is involved and thus is presented only in terms of its basic principles and primary results. The second method seems to be more intuitive, can be modified easily to treat general cases, and is discussed in more detail. We do not provide the derivation of all the equations from first principles and focus mainly on the technical aspects of solving the line shape problem in a general manner, and performing efficient parameter fitting. A "Matlab" routine that performs the numerical simulation is provided in the

Appendix (and can be obtained by e-mail from the corresponding author). This routine should help readers understand the fine details of the calculations, enabling "hands-on" experience with such simulative work.

TRIPLET LINE SHAPE SIMULATION

First we present the triplet spin Hamiltonian under consideration, which is given in the laboratory frame of reference by (12, 16)

$$\mathcal{H}(t) = g\beta\mathcal{S} \cdot B_0 + D\{\mathcal{S}_Z^2(t) - \tfrac{1}{3}\mathcal{S}(\mathcal{S} + 1)\}$$
$$+ E(\mathcal{S}_X^2(t) - \mathcal{S}_Y^2(t)) + \epsilon(t) \quad [1]$$

where

$$D = D_{ZZ} - \tfrac{1}{2}(D_{XX} + D_{YY}) \qquad [2]$$

$$E = \tfrac{1}{2}(D_{XX} - D_{YY}) \qquad [3]$$

$$\epsilon(t) = \tfrac{1}{2}g\beta B_1[S_+e^{-i\omega t} + S_-e^{+i\omega t}]. \qquad [4]$$

Here, D_{ii} are the components of the ZFS $\boldsymbol{D}$ tensor and $\mathcal{S}_i$ are the components of the triplet's spin operator, $\mathcal{S}$ (whose representation in the laboratory frame of reference depends on time due to possible triplet molecule rotations). The symbols $\mathcal{S}_\pm = (\mathcal{S}_x \pm i\mathcal{S}_y)$ are the Heisenberg raising $(+)$ and lowering $(-)$ spin operators in the laboratory frame of reference. We will treat only cases where the electronic exchange interaction J is large enough so that the triplet levels can be considered independently of the singlet level (16). In most of the relevant cases the triplets are distributed in some solvent or in a solid matrix. Therefore, we do not consider in our treatment g factor anisotropy or hyperfine terms, as they are seldom resolved in the inhomogenously broadened triplet spectra obtained for such cases (17). The case of single crystal spectra, where sharp lines are obtained, is unique in this respect (18). A good quantitative criteria for safely neglecting the g factor anisotropy, Δg, is $\Delta g B_0 \ll 1/T_2$ (the units of both sides are expressed commonly in Tesla). In a similar manner, the hyperfine interaction can be considered negligible if it is much smaller the native line width. Even if these criteria are not strictly met, in most cases one finds that $\Delta g B_0 \ll D$, and then the anisotropy can be effectively accounted for by an increased line broadening $(1/T_2)$ in the simulation without substantial loss of structural or dynamic molecular information. The CW microwave

radiation, which "probes" these spins and enables the detection of the EPR signal, is considered through the term $\epsilon(t)$. This radiation is assumed to be weak perturbation with respect to the other components of the spin Hamiltonian. Having defined the scope of our problem, we now calculate the triplet line shape, characterized by the above Hamiltonian. The line shape is normally measured in a specific microwave frequency, as a function of the applied field. However, it is more comfortable to calculate the line shape as a function of frequency for a given static magnetic field (which is just a mirror image of the experimental spectrum).

A general expression for the EPR line shape for the case of CW detection is given by (19, 20)

$$I(\omega) \propto \int_{-\infty}^{\infty} \text{Tr}\{\rho_0\mathcal{S}_+(0)\mathcal{S}_+(t)\}\sin(\omega t)dt \qquad [5]$$

where ρ_0 is the equilibrium density matrix. Thus, to calculate the line shape, one must find the time dependant $\mathcal{S}_+(t)$. In general, the operator time dependence is given by the solution of the equation (21)

$$\frac{\partial\mathcal{S}_+(t)}{\partial t} = -i[\mathcal{S}_+(t), \mathcal{H}(t)] \qquad [6]$$

where the Hamiltonian of Eq. [1] has explicit (usually stochastic) time dependence, due to the possible rotation of the triplet molecule.

One possible approach to solve Eq. [6] is to remove the explicit time dependence of the Hamiltonian using the method suggested by Kubo (22) and to obtain the stochastic Liouville equation (SLE) of motion (12):

$$\frac{\partial\mathcal{S}_+(\boldsymbol{\Omega}, t)}{\partial t} = -i[\mathcal{S}_+(\boldsymbol{\Omega}, t), \mathcal{H}(\boldsymbol{\Omega})] - \boldsymbol{\Gamma_\Omega}\mathcal{S}_+(\boldsymbol{\Omega}, t)$$
$$[7]$$

where $\boldsymbol{\Gamma_\Omega}$ is a stationary operator, satisfying the differential equation

$$\frac{\partial P(\boldsymbol{\Omega}, t)}{\partial t} = -\boldsymbol{\Gamma_\Omega}P(\boldsymbol{\Omega}, t) \qquad [8]$$

where $P(\boldsymbol{\Omega}, t)$ is the probability of finding a molecule at orientation $\boldsymbol{\Omega}$ at time t. After eliminating the explicit time dependence of the Hamiltonian, one can diagonalize the Liouville superoperator and then numerically solve Eq. [7] under various limiting condi-

tions (*12*, *23*). This method of solution is involved and difficult to generalize in the case of energy exchange (see below).

We employ here a different method and solve Eq. [6] by modeling the time dependence of the Hamiltonian through a set of coupled equations, each with a different time independent Hamiltonian. For example, if the Hamiltonian depends on time due to rotational motion of the molecule, we can account for such triplet tumbling by assuming the existence of *N* fictitious species. Each species has its own molecular orientation with respect to the external magnetic field, and the coupling between the equations can account for the molecular rotation. Thus, molecular rotation is treated not by a continuous rotation of a single species but as discrete jumps between species having different molecular orientations. Such discrete jumps, or any other process that changes abruptly the Hamiltonian, are denoted here as "exchange process" or simply exchange. We show (without a rigorous proof) that if the Hamiltonian is monotonically dependant on the molecular rotation around one of its axis, then in most cases such rotation can be accounted for by the exchange of just two species with different orientations with respect to the molecular axis of rotation. If one considers more involved rotations around two or three molecular axes, more species are needed to accurately represent such motion. Thus, in the case of monotonic Hamiltonian changes due to rotations around the three molecular axes, three species will be sufficient in most cases to accurately describe complex rotations. For a more involved Hamiltonian, with nonmonotonic behavior due to rotation, or for the case of very slow motion, one may add additional exchanging species (analogues to the requirement for larger basis sets in the solution of Eq. [7] for such cases (*12*)). Apart from its relative simplicity, the advantage of the method presented here is that more involved and generalized cases of exchange processes, with or without rotation, can be treated accordingly. In the most generalized case, each species may have its own ZFS parameters (*D* and *E*), anisotropic spin relaxation times (T_{1x}, T_{1y}, T_{1z}, T_{2x}, T_{2y}, T_{2z}), and anisotropic selective levels' population (A_x, A_y, A_z to the triplet X, Y, and Z levels, respectively) (*24*). In addition, each species may have its own orientation in the magnetic field. Thus, the exchange processes considered here can occur within the same molecular species undergoing "discrete jumps" between different possible orientations, and/or molecular interconversion of conformers, and/or between two physically different species undergoing intermolecular exchange. To summarize, in the most general case we solve a system of coupled equations where each equation relates to a specific different species, which can be a physically different molecule or the same molecule under different physical condition (different Hamiltonian).

Before we further present our method, we first account for relaxation mechanisms. In the formalism described by Eq. [7], relaxation mechanisms are "automatically" being accounted for by considering the continuous stochastic tumbling motion of the molecule, which is usually the dominant mechanism for spin-spin and spin-lattice relaxation in triplets (*2*). In our model, however, the Hamiltonian of each equation (describing a fixed molecular orientation) is time independent (disregarding the CW irradiation). Such formalism eliminates any possible relaxation mechanisms, as there is no stochastic time-dependant part in the Hamiltonian. Thus, to account for possible relaxation processes, a phenomenological Redfield relaxation superoperator, $\mathscr{R}$, is added to Eq. [6] (*20*, *25*), while the Hamiltonian is still kept constant (but still depends on orientation)

$$\frac{\partial \mathscr{S}_+(t)}{\partial t} = -i[\mathscr{S}_+(t), \mathscr{H}(\mathbf{\Omega})] + \mathscr{R}\mathscr{S}_+(t) \quad [9]$$

Equation [9] was originally obtained by Redfield with the assumption that the main Hamiltonian (which appears in the commutator) is time independent and there is an additional small stochastic time dependant term, which is expressed through the relaxation term $\mathscr{R}$. Here the same formal equation is employed, which accounts for any unknown relaxation mechanism, in the presence of a fixed Hamiltonian. The relaxation operator employed here contains only elements of transverse relaxation (T_2), which affect the line shape, but ignores the effects of longitudinal relaxation (T_1), which affects the line shape only indirectly through the levels' population. These populations are considered in the line shape calculations (Eq. [5]) through ρ_0 (see below).

With the formalism stated above, Eq. [9] can be written separately for each different species (*A, B, ..*), with the addition of an exchange term, which couples all the equations together (*20*):

$$\frac{\partial \mathscr{S}_+^A(t)}{\partial t} = -i[\mathscr{S}_+^A(t), \mathscr{H}^A] + \sum_B (P_{AB}\mathscr{S}_+^A(t)$$

$$- P_{BA}\mathscr{S}_+^A(t)) + \mathscr{R}\mathscr{S}_+^A(t) \quad [10]$$

where P_{AB} is the rate of exchange between species *A* to *B* and so forth. This set of equations can be written in a compact form by using the appropriate superoperators

$$\frac{\partial \hat{\mathscr{G}}_+(t)}{\partial t} = -i(\hat{\mathbf{\Omega}} - i\hat{\mathbf{\Pi}} + \hat{\mathscr{R}})\hat{\mathscr{G}}_+(t) \qquad [11]$$

where $\hat{\mathscr{G}}_+$ is an operator, which represents all the exchanging species (see below). The superoperator $\hat{\mathbf{\Omega}}$ corresponds to the operator $[\mathscr{G}_+^i(t), H^i]$ in Eq. [10] for the entire N exchanging species (with the dimension of $9N \times 9N$). The superoperators $\hat{\mathbf{\Pi}}$ and $\hat{\mathscr{R}}$ are related to the exchange and the relaxation processes, respectively, and are described below. Equation [11] has the formal solution

$$\hat{\mathscr{G}}_+(t) = \exp[i(\hat{\mathbf{\Omega}} + i\hat{\mathbf{\Pi}} + \hat{\mathscr{R}})t]\hat{\mathscr{G}}_+ \qquad [12]$$

With this solution, one can continue and follow the approach of Hudson and McLachlan (20), which relies on the extensive treatment of Kubo and Tomita (26), and Alexander (15, 27) to write Eq. [5] for the line shape intensity I versus ω, for a given DC field as

$$I(\omega) = 2 \text{ Im Tr}\left\{\rho_0\hat{\mathscr{G}}_+\left[\frac{1}{(\hat{\mathbf{\Omega}} - \omega - i(\hat{\mathbf{\Pi}} + \hat{\mathscr{R}}))}\right]\hat{\mathscr{G}}_+\right\}$$
$$[13]$$

where ρ_0 is the density matrix operator describing all the species (detailed below). In the original treatment (20), ρ_0 describes the thermal triplet population. However, in the general case it should account for the possibility of a spin-polarized triplet.

We now proceed from the general theoretical introduction to the main part of this article, which presents a hands-on approach to the line shape simulation problem. To solve Eq. [13], one should describe explicitly the matrix form of $\hat{\mathbf{\Omega}}$, $\hat{\mathbf{\Pi}}$ and $\hat{\mathscr{R}}$. These matrices provide the denominator of Eq. [13], which can then be obtained through a numerical matrix inversion. The inverted matrix is then multiplied by the supervectors, representing $\hat{\mathscr{G}}_+$ and ρ_0, to obtain the line shape relative intensity at frequency ω. First, one must determine the vector basis set, by which the supervectors and supermatrices are represented. To simplify the problem, we diagonalize the full Hamiltonian by using a standard procedure in which first D and E are neglected (they are usually at least ~ 10 times smaller than the Zeeman interaction, for X-band measurements) to obtain the eigenvectors from the high-field wave functions, $|-1>$, $|0>$, $|1>$ (28):

$$\begin{pmatrix}\Sigma_1 \\ \Sigma_2 \\ \Sigma_3\end{pmatrix} = \begin{pmatrix} \frac{1}{2}(l - im)\left[\frac{1+n}{1-n}\right]^{1/2} & \sqrt{2}(1-n^2)^{1/2} & \frac{1}{2}(l+im)\left[\frac{1-n}{1+n}\right]^{1/2} \\ -\sqrt{2}(l-im) & n & \sqrt{2}(l+im) \\ \frac{1}{2}(l-im)\left[\frac{1-n}{1+n}\right]^{1/2} & -\sqrt{2}(1-n^2)^{1/2} & \frac{1}{2}(l+im)\left[\frac{1+n}{1-n}\right]^{1/2} \end{pmatrix} \begin{pmatrix} |1> \\ |0> \\ |-1> \end{pmatrix} \qquad [14]$$

Following this, D and E are accounted for as a first-order perturbation, to obtain the diagonal Hamiltonian

matrix (28):

$$H = \begin{bmatrix} -\frac{D}{6}(1 - 3n^2) + \frac{E}{2}(l^2 - m^2) + \omega_0 & 0 & 0 \\ 0 & \frac{D}{3}(1 - 3n^2) - E(l^2 - m^2) & 0 \\ 0 & 0 & -\frac{D}{6}(1 - 3n^2) + \frac{E}{2}(l^2 - m^2) - \omega_0 \end{bmatrix}$$
$$[15]$$

where $l = \sin\theta\,\cos\phi$; $m = \sin\theta\,\sin\phi$; and $n = \cos\theta$, for the spatial angle θ, ϕ, which describe the direction of B_0 with respect to the molecular Z axis (Fig. 2[a]), and $\omega_0 = g\beta B_0$. Thus, as expected, the three energy levels depend on the molecular orientation in the external magnetic field, resulting in a broad inhomogeneous spectrum for isotropically distributed molecular orientations. To explicitly describe $\mathbf{\Omega}$ (the supermatrix form of $\hat{\mathbf{\Omega}}$), we write in detail how this operator operates on a general matrix v.

$$
\Omega^A v = [\mathcal{H}^A,\, v] = \mathcal{H}^A v - v\mathcal{H}^A =
\begin{bmatrix} H_{11}^A & 0 & 0 \\ 0 & H_{22}^A & 0 \\ 0 & 0 & H_{33}^A \end{bmatrix}
\begin{bmatrix} v_{11} & v_{12} & v_{13} \\ v_{21} & v_{22} & v_{23} \\ v_{31} & v_{32} & v_{33} \end{bmatrix}
-
\begin{bmatrix} v_{11} & v_{12} & v_{13} \\ v_{21} & v_{22} & v_{23} \\ v_{31} & v_{32} & v_{33} \end{bmatrix}
\begin{bmatrix} H_{11}^A & 0 & 0 \\ 0 & H_{22}^A & 0 \\ 0 & 0 & H_{33}^A \end{bmatrix}
$$

$$
=
\begin{bmatrix} H_{11}^A v_{11} & H_{11}^A v_{12} & H_{11}^A v_{13} \\ H_{22}^A v_{21} & H_{22}^A v_{22} & H_{22}^A v_{23} \\ H_{33}^A v_{31} & H_{33}^A v_{32} & H_{33}^A v_{33} \end{bmatrix}
-
\begin{bmatrix} H_{11}^A v_{11} & H_{22}^A v_{12} & H_{33}^A v_{13} \\ H_{11}^A v_{21} & H_{22}^A v_{22} & H_{33}^A v_{23} \\ H_{11}^A v_{31} & H_{22}^A v_{32} & H_{33}^A v_{33} \end{bmatrix}
$$

$$
=
\begin{bmatrix} 0 & (H_{11}^A - H_{22}^A)v_{12} & (H_{11}^A - H_{33}^A)v_{13} \\ (H_{22}^A - H_{11}^A)v_{21} & 0 & (H_{22}^A - H_{33}^A)v_{23} \\ (H_{33}^A - H_{11}^A)v_{31} & (H_{33}^A - H_{22}^A)v_{32} & 0 \end{bmatrix}
\quad [16]
$$

Thus, the commutator can be represented in a supermatrix form as

$$
\Omega^A v = [\mathcal{H}^A,\, v] =
\begin{bmatrix}
0 & 0 & 0 & 0 & 0 & 0 & 0 & 0 & 0 \\
0 & H_{11}^A - H_{22}^A & 0 & 0 & 0 & 0 & 0 & 0 & 0 \\
0 & 0 & H_{11}^A - H_{33}^A & 0 & 0 & 0 & 0 & 0 & 0 \\
0 & 0 & 0 & H_{22}^A - H_{11}^A & 0 & 0 & 0 & 0 & 0 \\
0 & 0 & 0 & 0 & 0 & 0 & 0 & 0 & 0 \\
0 & 0 & 0 & 0 & 0 & H_{22}^A - H_{33}^A & 0 & 0 & 0 \\
0 & 0 & 0 & 0 & 0 & 0 & H_{33}^A - H_{11}^A & 0 & 0 \\
0 & 0 & 0 & 0 & 0 & 0 & 0 & H_{33}^A - H_{22}^A & 0 \\
0 & 0 & 0 & 0 & 0 & 0 & 0 & 0 & 0
\end{bmatrix}
\begin{bmatrix} v_{11} \\ v_{12} \\ v_{13} \\ v_{21} \\ v_{22} \\ v_{23} \\ v_{31} \\ v_{32} \\ v_{33} \end{bmatrix}
$$

$$[17]$$

If the Hamiltonian (Eq. [15]) was not diagonal, the resulting supermatrix would have been much more complicated, but the same formalism would still be valid. The supermatrix Ω^A in Eq. [17] is for one species only, the total supermatrix $\mathbf{\Omega}$ is with dimension of $9N \times 9N$, where the supermatrices $\Omega^{A,B,C..}$ are on the diagonal of the large banded $\mathbf{\Omega}$ supermatrix.

$$
\mathbf{\Omega}v =
\begin{bmatrix}
\Omega^A & 0 & 0 & \cdots \\
0 & \Omega^B & 0 & \cdots \\
0 & 0 & \Omega^C & \cdots \\
\cdots & \cdots & \cdots & \cdots
\end{bmatrix}
\begin{bmatrix} v^A \\ v^B \\ v^C \\ \cdots \end{bmatrix}
\quad [18]
$$

The banded form of $\mathbf{\Omega}$ is due to the assumption that each Hamiltonian acts on each species separately, without mutual interaction (apart for the exchange, which is considered separately). Equations [17] and [18] show the explicit representation of the operator $\hat{\mathbf{\Omega}}$ in Eq. [13], which is used below to obtain the numerical solution.

The supermatrix $\hat{\mathbf{\Pi}}$ can also be written in an explicit from. For example, consider the case of a system with three sites, exchanging between themselves with rates denoted by P_{12}, P_{21}, P_{13}, P_{31}, P_{23},
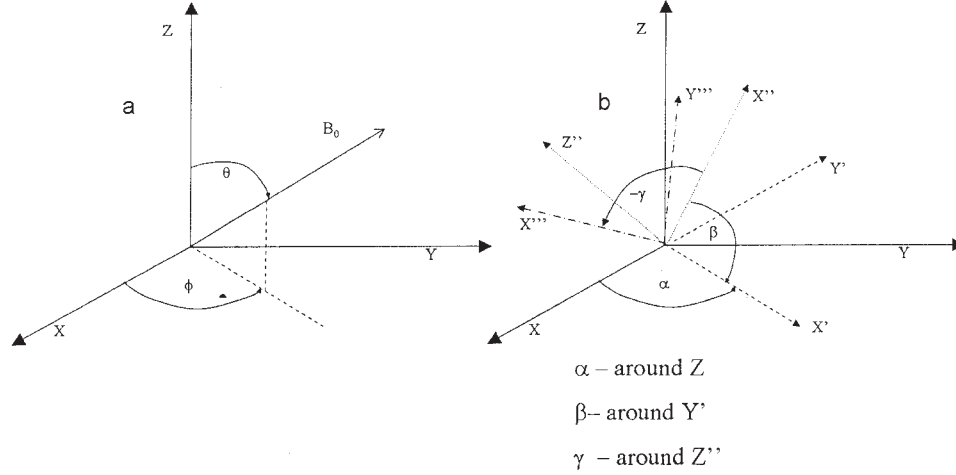
Figure 2   (a) Coordinate system used in this article. The XYZ axes represent the triplet's molecular frame of reference and B_0 is the direction of the external magnetic field with respect to this axes system. (b) Euler angles used to represent molecular change of orientation (i.e., exchange between two species or rotation). Starting from the system XYZ, a rotation by angle α around the Z axis results in the system X'Y'Z (dashed). Consequently, a rotation by an angle β around the new Y' axis results in the system X"Y'Z" (dotted). Finally a rotation by an angle γ around the new Z" axis results in the system X"'Y"'Z" (dashed dotted).

and P_{32}. In this case, the exchange superoperator $\hat{\Pi}$ is written as

$$\hat{\Pi} = \begin{bmatrix} -P_{12} - P_{13} & P_{21} & P_{31} \\ P_{12} & -P_{21} - P_{23} & P_{32} \\ P_{13} & P_{23} & -P_{31} - P_{32} \end{bmatrix} \quad [19]$$

Here, each term in this matrix represents a diagonal 9×9 matrix, and the overall size of the supermatrix $\hat{\Pi}$ is a 27×27, which affects all the spin matrix components of the three species. Equation [19] can be generalized to the case of N interacting species:

$$\hat{\Pi} = \begin{bmatrix} -P_{12} - P_{13} - \cdots P_{1N} & P_{21} & P_{31} & \cdots & P_{N1} \\ P_{12} & -P_{21} - P_{23} - \cdots P_{2N} & P_{32} & \cdots & P_{N2} \\ P_{13} & P_{23} & -P_{31} - P_{32} - \cdots P_{3N} & \cdots & P_{N3} \\ \cdots & \cdots & \cdots & \cdots & \cdots \\ P_{1N} & P_{2N} & P_{3N} & \cdots & -P_{N1} - P_{N2} - \cdots P_{N(N-1)} \end{bmatrix} \quad [20]$$

Here the overall size of the supermatrix $\hat{\Pi}$ is $9N \times 9N$. This matrix will be employed in the numerical solution of Eq. [13] (see below).

The relaxation superoperator $\hat{\mathcal{R}}_i$ is related in our treatment only to the spin-spin relaxation time T_{2i} (of species i), while T_1 is taken into account through ρ_0 (in Eq. [5]). The general expression for

T_{2i}, for a specific molecular orientation (described by m,n,l), can be obtained by means of the anisotropic values of T_{2ix}, T_{2iy}, and T_{2iz} at the canonical orientations (4)

$$T_{2i,l,m,n} = T_{2ix}l^2 + T_{2iy}m^2 + T_{2iz}n^2. \quad [21]$$

Because T_2 mechanisms act only on the transverse magnetization, the supermatrix $\mathbf{R_i}$ is constructed such that only the off-diagonal elements of $\mathcal{S}^i_+$ are affected:

$$\mathbf{R_i} = \begin{vmatrix} 0 & 0 & 0 & 0 & 0 & 0 & 0 & 0 & 0 \\ 0 & 1/T_{2i,l,m,n} & 0 & 0 & 0 & 0 & 0 & 0 & 0 \\ 0 & 0 & 1/T_{2i,l,m,n} & 0 & 0 & 0 & 0 & 0 & 0 \\ 0 & 0 & 0 & 1/T_{2i,l,m,n} & 0 & 0 & 0 & 0 & 0 \\ 0 & 0 & 0 & 0 & 0 & 0 & 0 & 0 & 0 \\ 0 & 0 & 0 & 0 & 0 & 1/T_{2i,l,m,n} & 0 & 0 & 0 \\ 0 & 0 & 0 & 0 & 0 & 0 & 1/T_{2i,l,m,n} & 0 & 0 \\ 0 & 0 & 0 & 0 & 0 & 0 & 0 & 1/T_{2i,l,m,n} & 0 \\ 0 & 0 & 0 & 0 & 0 & 0 & 0 & 0 & 0 \end{vmatrix} \qquad [22]$$

The full supermatrix $\hat{\mathbf{R}}$ may take into account different relaxation rates for the different species and is constructed from the individual $\mathbf{R_i}$. Thus, for example, in the case of three species, $\hat{\mathbf{R}}$ has dimensions of 27×27 and can be represented by

$$\hat{\mathbf{R}} = \begin{pmatrix} (\mathbf{R}_1) & 0 & 0 \\ 0 & (\mathbf{R}_2) & 0 \\ 0 & 0 & (\mathbf{R}_3) \end{pmatrix} \qquad [23]$$

This expression can be generalized to the case of N interacting species. Again, the $\hat{\mathbf{R}}$ matrix is used below in the explicit numerical solution of Eq. [13].

The final issue to be addressed before calculating the line shape with Eq. [13] is the supervector ρ_{0i}, which represents the triplet level's population of species i. The individuals ρ_{0i} are later used to obtain ρ_0, which accounts for the energy levels' population of all species. Although in general, ρ_{0i} contains nine different elements for each triplet species, in the case of CW detection, only matrix elements, which correspond to the coherence generated between levels 1 and 2 of the triplet and levels 2 and 3 of the triplet (under high magnetic field), are important for the line shape calculation (5). Thus, for the case of thermal triplets, ρ_{0i} can be taken as:

$$\rho_{0i} = \begin{pmatrix} 0 & 1 & 0 \\ 0 & 0 & 1 \\ 0 & 0 & 0 \end{pmatrix} \qquad [24]$$

which means that the population difference between levels 1 and 2 is (almost) equal to the population difference between levels 2 and 3. For photoexcited triplets, with spin polarization, the population differ-

ence between the levels is far from being equal. In this case, one can determine ρ_{0i} from the information about the selective levels' population of the triplet's principle levels, A_x, A_y, A_z for each of the species (6, 29). Due to the origin of the spin polarization, the triplet levels' population depends on the orientation of the molecule with respect to the external magnetic field. To properly account for this effect, we first examine the population difference of the two allowed EPR transitions in the three canonical orientations. We also consider the decay of the triplet levels' population to thermal equilibrium following the laser pulse that generates the polarized triplets (6). For example, in a situation where the triplet's molecular X axis is parallel to the magnetic field, the population difference, corresponding to the two EPR transitions for species i, will be (6, 29)

$$\Delta_{x1}^i = (-\alpha_x^i + \beta_x^i)e^{-3t/T_{1x}^i} + \Delta_{eq}(1 - e^{-3t/T_{1x}^i}) \qquad [25]$$

$$\Delta_{x2}^i = (\alpha_x^i + \beta_x^i)e^{-3t/T_{1x}^i} + \Delta_{eq}(1 - e^{-3t/T_{1x}^i}) \qquad [26]$$

where the parameters α_x^i and β_x^i of species i are obtained through simple expression from A_x^i, A_y^i, A_z^i (29); T_{1x}^i is the spin lattice relaxation (SLR) time of the triplet for the X canonical orientation, and Δ_{eq} is the thermal equilibrium population difference. (Thus, the thermal population case is obtained for t → ∞.) Similarly, $\Delta_{y1}^i, \Delta_{y2}^i, \Delta_{z1}^i,$ and Δ_{z2}^i can be calculated for the other canonical orientations. The population differences in the canonical orientations are used to obtain the population difference in any arbitrary orientation, which is described by the parameters l,m,n (see Fig. 2), using the expressions (4)
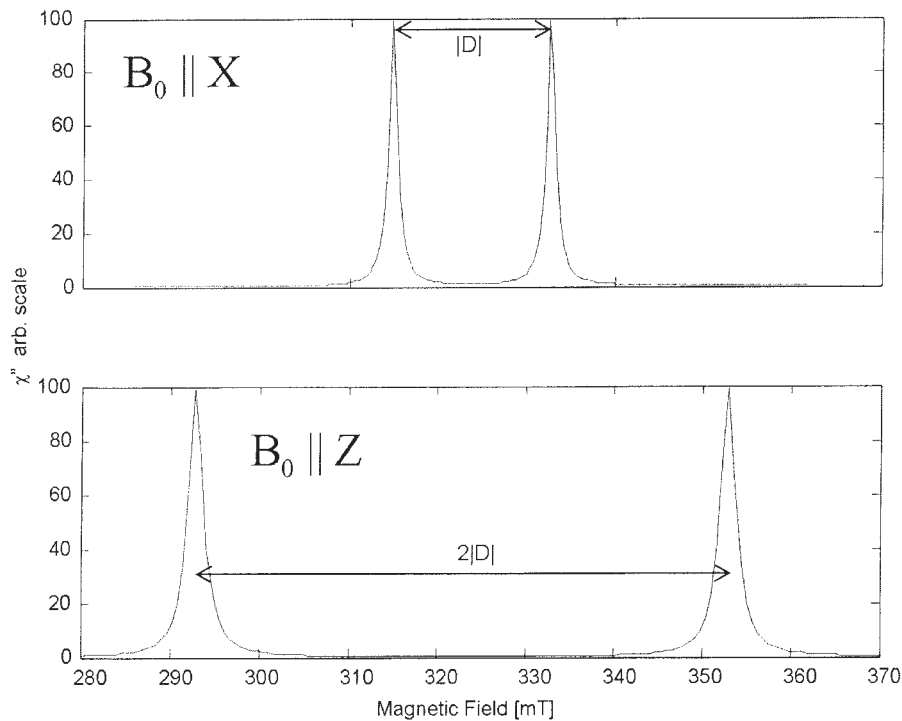
Figure 3 Theoretical calculations (X-band frequency) of the triplet EPR line shape for a single molecular orientation. Top: $B_0 \parallel X$; bottom: $B_0 \parallel Z$. The triplet parameters for these calculations are $D = 30$ mT; $E = 0$; $1/T_2 = 1$ mT (for all molecular axes). The line shape pattern for $B_0 \parallel Y$ is identical to $B_0 \parallel X$ because $E = 0$. The triplet is in thermal equilibrium (positive sign corresponds to absorption signal).

$$\Delta_{l,m,n1}^{i} = \Delta_{x_1}^{i} l^2 + \Delta_{y_1}^{i} m^2 + \Delta_{z_1}^{i} n^2 \qquad [27]$$

$$\Delta_{l,m,n2}^{i} = \Delta_{x_2}^{i} l^2 + \Delta_{y_2}^{i} m^2 + \Delta_{z_2}^{i} n^2 \qquad [28]$$
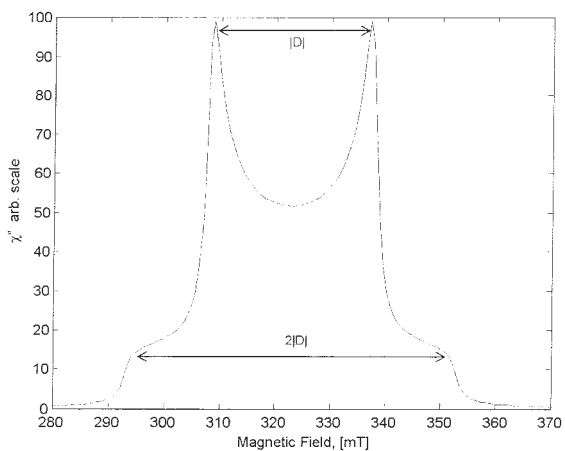

Figure 4 Calculated triplet EPR line shape for randomly oriented thermal triplet molecules. Triplet parameters are: $D = 30$ mT; $E = 0$; $1/T_2 = 1$ mT.
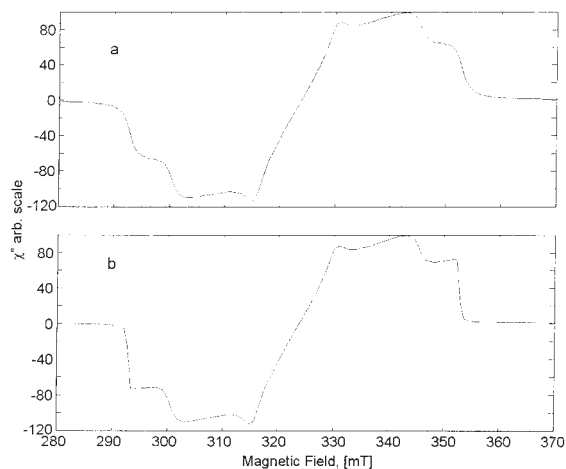

Figure 5 (a) Calculated EPR line shape for polarized triplet ($A_x = A_y = 1$; $A_z = 0$) with the parameters $D = 30$ mT; $E = 5$ mT; $1/T_{2x} = 1/T_{2y} = 1/T_{2z} = 1$ mT. (b) The same calculation, but assuming anisotropic relaxation rates $1/T_{2y} = 1/T_{2y} = 1$mT; $1/T_{2z} = 0.1$ mT. Positive sign corresponds to absorption signal; negative sign corresponds to emission signal.
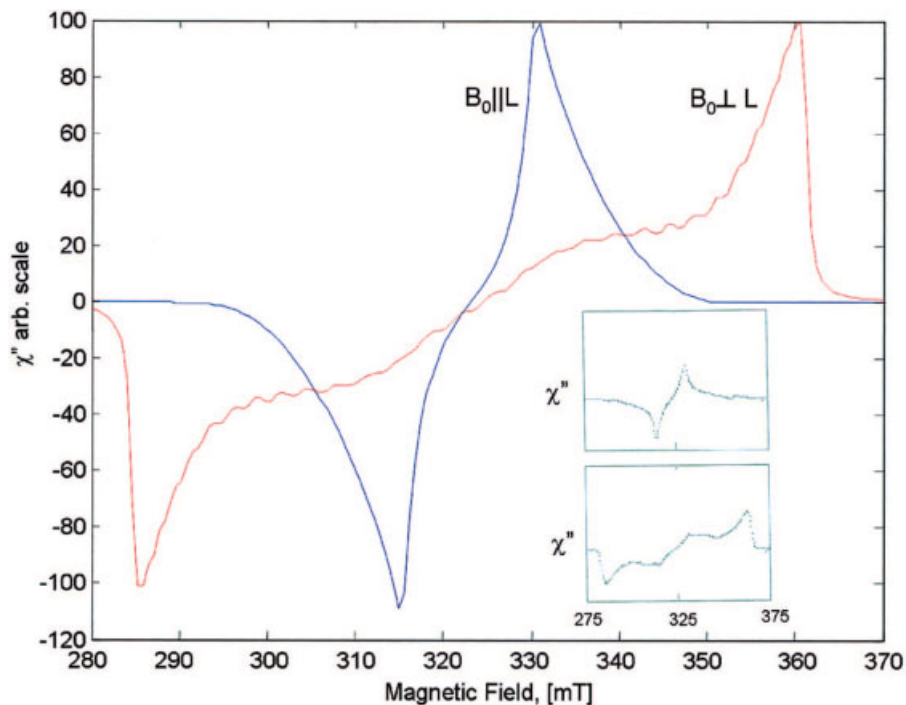
Figure 6   Calculated triplet line shape for the case of anisotropic frozen solvent. Triplet parameters are $D = 35$ mT; $E = 6$ mT; $1/T_2 = 1$ mT; (B $\parallel$ L; B $\perp$ L). Results can be qualitatively compared to a similar experimental case shown in the small legend on the right (borrowed with permission from (*14*)). Positive sign corresponds to absorption signal; negative sign corresponds to emission signal. [Color figure can be viewed in the online issue, which is available at www.interscience. wiley.com.]

This formalism can be performed for each of the species separately, thus allowing for the consideration of different population rates for each species. The population difference between the levels is used for the construction of ρ_{0i}:

$$\rho_{0i} = \begin{pmatrix} 0 & \Delta^i_{l,m,n2} & 0 \\ 0 & 0 & \Delta^i_{l,m,n1} \\ 0 & 0 & 0 \end{pmatrix} \qquad [29]$$

This matrix may be different for each of the species and can be incorporated to construct the full ρ_0 supervector:

$$\rho_0 = (0 \quad \Delta^1_{l,m,n2} \quad 0 \quad 0 \quad 0 \quad \Delta^1_{l,m,n1} \quad 0 \quad 0 \quad 0 \quad 0$$
$$\Delta^2_{l,m,n2} \quad 0 \quad 0 \quad 0 \quad \Delta^2_{l,m,n1} \quad 0 \quad 0 \quad 0 \cdots) \quad [30]$$

Where we "broke" the ρ_{0i} matrix into a supervector form and then cascaded all the vectors to a single supervector. This super vector will be used in the numerical solution of Eq. [13].

Having explicitly calculated and presented all the relevant supermatrices and supervectors appearing in Eq. [13], one can numerically invert the supermatrix in the denominator of Eq. [13] and obtain the line shape $I(\omega)$ for any given ω and molecular orientation (l, m, n). The final line shape is obtained by the numerical integration of $I(\omega)$ over all the possible molecular orientations:

$$I^{total}(\omega) = \int_\theta \int_\phi P(\theta, \phi) I(\omega, \theta, \phi) d\phi d\theta \qquad [31]$$

where $P(\theta,\phi)$ is the distribution function of the molecular orientations. For example, in the case of isotropic solvents, $P(\theta,\phi)$. In the case of anisotropic solvents (e.g., liquid crystals, LCs), the distribution function is usually more complicated (*4*, *14*).

APPLICATIONS AND EXAMPLES

The theory discussed above was implemented in a short "Matlab" routine (see Appendix), which calculates the triplet EPR line shape in many cases of interest. We now
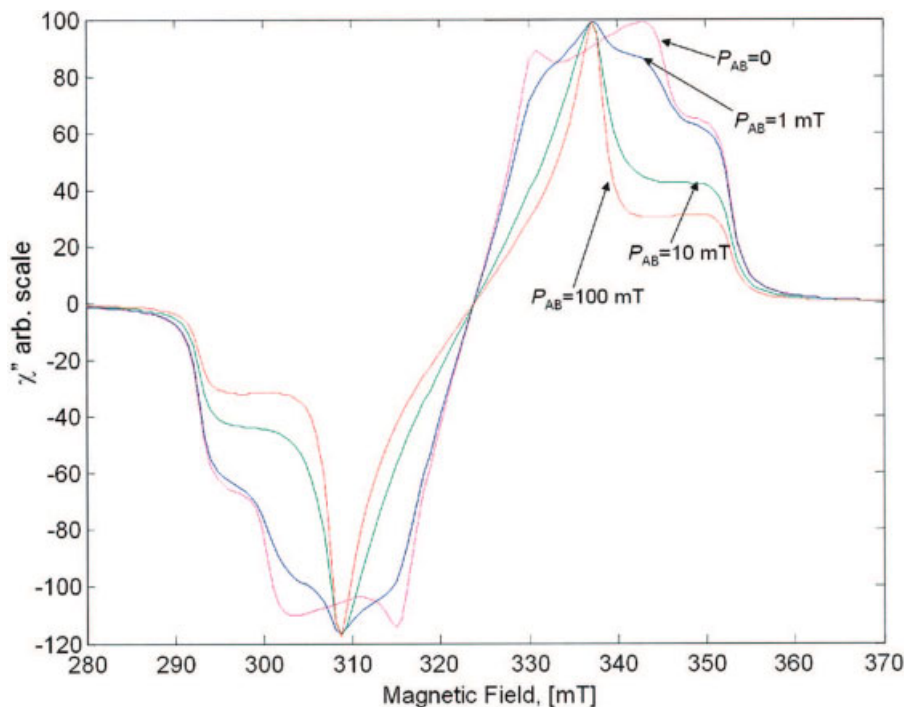
Figure 7 Calculated triplet EPR line shape for polarized triplet ($A_x = A_y = 1$; $A_z = 0$) with parameters $D = 30$ mT; $E = 5$ mT; $1/T_{2x} = 1/T_{2y} = 1/T_{2z} = 1$ mT. The triplet molecule undergoes rotation around the molecular Z axis with increasing rate. The rotation is modeled as an exchange between two species with relative Euler angles $(\alpha,\beta,\gamma) = (90,0,0)$ and exchange rate P_{AB}. Positive sign corresponds to absorption signal; negative sign corresponds to emission signal. [Color figure can be viewed in the online issue, which is available at www.interscience.wiley.com.]

describe several examples of these theoretical calculations, ranging from simple to complex cases.

We begin by looking at a "synthetic example" of a single species in thermal equilibrium, where the magnetic field is positioned along the X or Z axis of the triplet molecule (Fig. 3). This case results in a simple single crystal-like spectrum, where the distance between the two peaks in the Z-axis orientation equals $2D$, as expected (*1*).

In the next example, we still consider only single species and assume an isotropic solvent where the line shape is the summation of all randomly distributed triplet molecules (Fig. 4). The resulting line shape is the well-known Pake doublet (*1, 30*).

Next, we consider the case of a spin polarized triplet (single species), where the ZFS parameters D, $E \neq 0$ (Fig. 5[a]). The emission/absorption pattern obtained in this case is typical to $D > 0$, with the population of the triplet X and Y levels considered here (*14*). Note also that the spectrum is not completely antisymmetric, due to the net emissive polarization of the triplet (as expected for this selective population scheme (*24*)). Figure 5(b) shows the same spectrum, but for the case of anisotropic relaxation

rates T_2. Note that the relatively long T_2 for B ∥ Z causes the edges of the spectrum to become sharper.

From synthetic calculations we turn to simulations of actual measured spectra. Here we return to the spectrum showed earlier in Fig. 1. It presents the line shape of a triplet gallium-pentafluorophenylcorrole (Ga(tpfc)) in toluene. This is a unique example where the ZFS parameter D is negative as a result of molecular distortion and head-to-tail spin alignment (*3, 31*).

The next example is of an anisotropic solvent. Anisotropic environments are common in many biological and liquid crystalline systems (*32*). As mentioned earlier, the specific nature of the solvent (isotropic/anisotropic) is considered in the line shape calculation through the distribution function in Eq. [31]. The exact nature of this function depends on the specific properties of the solvent. Thus, the distribution of the molecular orientation in the laboratory frame of reference (Eq. [31]) is derived by first describing the distribution function of the molecules in the LCs frame of reference and then translating it to the distribution in the laboratory frame of reference. Figure 6 shows a line shape pattern typical for anisotropic distribution of planar triplet molecules in LC environment (*14, 33*).

As discussed above, molecular rotation can be accounted in the simulation by considering two or more exchanging species. As a first example, we calculate the spectrum of a triplet with the same parameters as in Fig. 5(a), which rotates around the molecular Z axis. This rotation is simulated as an exchange process between two species with different Hamiltonians (in this case, differing only by the relative orientation of the triplet with respect to B_0). The relation between the orientations of the two species can be described by means of the Euler angles. A common definition of the Euler angles is shown in Fig. 2(b). Thus, for example, rotation around the molecular Z axis can be described by the Euler angles $(\alpha,\beta,\gamma) = (90,0,0)$, where the rate of exchange between the species (the parameter P_{AB} in Eq. [10]) provides the rotational correlation time for such rotation through the relation

$$\tau_c = \frac{2}{\pi P_{AB}} \qquad [32]$$

Therefore, if one considers a 90° "jump" process, at exchange rate P_{AB}, it corresponds to molecular rotation at a rate of $\pi/2 \times P_{AB}$ radians/s. The spectrum, originating from such rotation for several values of P_{AB}, is shown in Fig. 7. It is evident that such rotation effectively averages out the E value.

Next, we consider a more complicated 3D rotation, as encountered in triplet C_{60} in fluid phases (13, 33). This spectrum can be simulated by examining three exchanging species related to each other by the Euler angles (90,90,0) and (0,90,90). Combining together these three species is equivalent to an isotropic rotation. Figure 8 presents the simulated results, compared with results obtained through the rotational diffusion model (13). The rigid limit and the motional narrowed spectrum give similar results with the two methods. For the slow rotation case, shown in Fig. 8(a) (central spectrum), there is a slight disagreement between the results of the two

methods. This is because the slow rotation spectrum cannot be described accurately as 90° jumps and should be considered through smaller discrete jumps. This implies that more than three exchanging species are required to accurately account for such conditions. One can qualitatively describe this requirement for increased number of exchanging species in an analogous manner
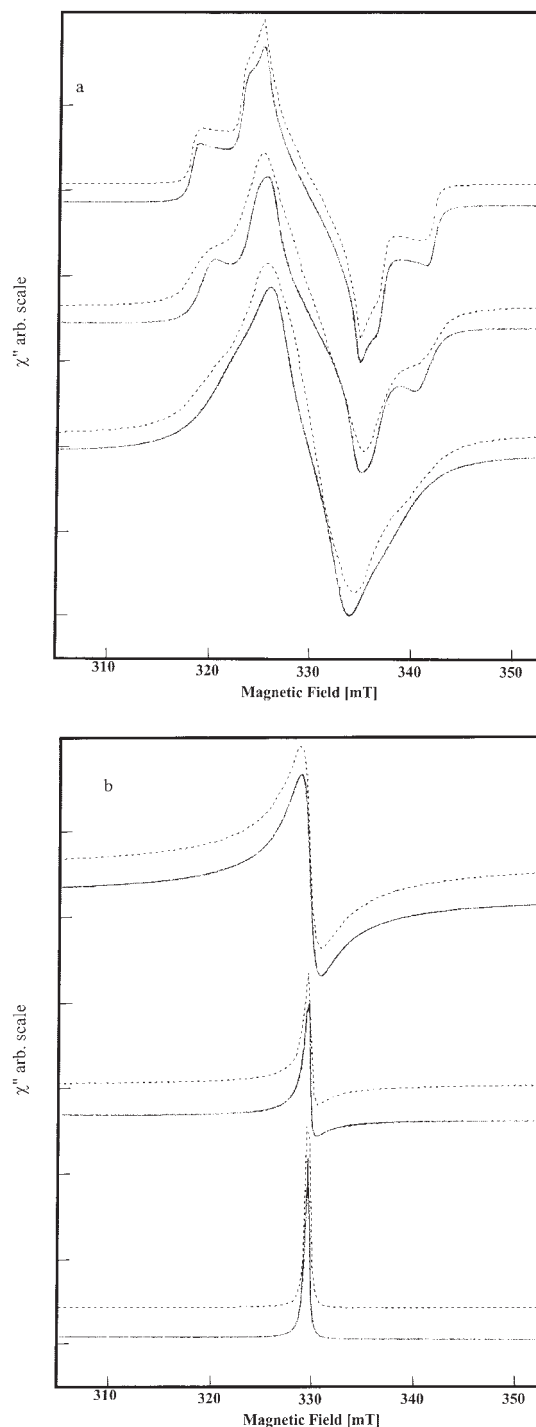

Figure 8   Calculated EPR line shape for photoexcited triplet C_{60} employing the rotational diffusion model (solid line; borrowed with permission from (13)), and the model presented here (dashed line). Calculation parameters $D = 11.4$ mT; $E = 0.69$ mT; $A_x = A_y = 0$; $A_z = 1$, $1/T_2 = 0.2$ mT. (a) Rotational diffusion calculation for slow rotation rate of $R = 10^6, 10^7, 10^8 \text{ s}^{-1}$ from top to bottom respectively, and exchange rate between the three sites of $P_{AB} = P_{AC} = P_{BC} = 3.3 \times 10^5, 3.3 \times 10^6, 3.3 \times 10^7$ from top to bottom respectively. (b) The same as (a) but for faster motion with $R = 10^9, 10^{10}, 10^{11} \text{ s}^{-1}$ and $P_{AB} = P_{AC} = P_{BC} = 3.3 \times 10^8, 3.3 \times 10^9, 3.3 \times 10^{10} \text{ s}^{-1}$, from top to bottom respectively. Positive sign corresponds to absorption signal while negative sign corresponds to emission signal.
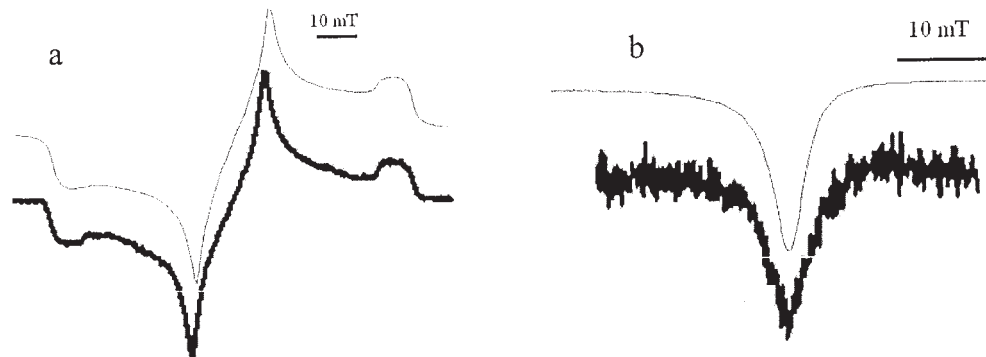
Figure 9 Simulated (upper trace) and measured (lower trace) triplet EPR line shape for photo-excited H$_2$TPP in toluene (Prof. S. Yamauchi, unpublished results). (a) Results for 25 K, $A_x = 1$; $A_y = 0.3$; $A_x = 0.3$; $D = 40.4$ mT; $E = 8$ mT, no molecular rotation. (b) Results for 300 K, the same parameters as in (a) but with molecular rotation simulated by three orthogonal exchanging species (as in the C$_{60}$ case), with exchange rate of $P_{AB} = P_{AC} = P_{BC} = 5 \times 10^9$ s^{-1}.

to the requirement of increased number of basis sets or finite difference divisions when solving similar problems (the stochastic Liouville equation) by means of the eigen value and the finite difference methods (*34*). In most cases, three species are enough to represent 3D rotations, but for slow rotations or more involved angular dependence of the Hamiltonian, one may require additional species to better simulate the experimental spectrum.

In the next example we consider a more complicated case, where the triplet molecule has two conformers undergoing interconversion and also rotates in solid or fluid solutions. Such cases occur, for example, for the photoexcited triplet state of boron subphthalocyanine chloride (*35*). The two molecular conformers have similar *D* but different *E* values. Using our present method, we could account for different population rates, different anisotropic relaxation rates, and even different rotation rates for the two molecular conformers. The experimental and the simulated results were presented in details in (*35*). The original discussion of these results (*35*) assumed that the absorption Lorentzian-like line shape appearing at high temperatures is mainly due to thermal relaxation (SLR). Such explanation provided good fit to the experimental results but does not account for emissive spectra found under similar conditions in triplets such as H$_2$TPP and MgTPP (*36*). An alternative explanation for the apparent thermalization of the spectrum is through very fast rotations about all the molecular axes, similar to the mechanism employed earlier for the C$_{60}$ case (*13*). Such process can be treated by the present line shape simulation, and it predicts a collapse of the triplet spectrum to single Lorentzian line, which can be either in absorption (as in the boron subphthalocyanine chloride case) or in emission (as in the case of the triplet of free-base porphyrin, H$_2$TPP (*36*)). Figure 9 shows typ-ical simulated and measured results of H$_2$TPP and a collapse of the spectrum to a single Lorentzian line in enhanced emission due to fast rotations.

CONCLUSIONS

We presented a general theory for the quantitative analysis of triplet EPR line shapes. The theory can be employed to extract from the experimental line shape a wide variety of parameters related to the triplet molecule. The theoretical basis for the line shape analysis was reviewed in detail, and several examples of calculated and measured results were provided. These examples demonstrate the ability to investigate cases such as triplets in solid solution with anisotropic relaxation and population, rotating triplets in liquid, exchange between different triplets, and a combination of exchange, rotation, and anisotropic relaxation and triplet level's population. A "Matlab" routine is provided to facilitate easier understanding of the various numerical issues involved in the line shape calculation and to enable simpler adoption of these theoretical tools by the readers.

ACKNOWLEDGMENTS

APPENDIX: "MATLAB" ROUTINE FOR LINE SHAPE SIMULATION

```
function [XXX, YYY]=triplet_line(c);
    % Matlab Ver. 6.1 with Symbolic Toolbox
    % This routine uses the +1 0 −1 wavefunctions
    % c is a vector containing the species parameters
    % X, Y the simulated EPR spectrum
    Np=200; % Number of points in the magnetic field calculation, a parameter.
    % The structure of c is fitted to up to 4 species, but the program is
    % generic to any number of species.
    % Input example
    if nargin==0,
    % c(1,1) % sample rotation angle - related to LC, not implemented here
    % c(1,2) % Sigma_theta(deg) - related to LC, not implemented here
    % c(1,3) % Phi_0 (deg) - related to LC, not implemented here
    % c(1,4) % Sigma phi_0 (deg) - related to LC, not implemented here
    c(1,5)=−316; % D (gauss), Site 1
    c(1,6)=67.3; % E (gauss), Site 1
    c(1,7)=100; % Percent, Site 1
    % c(1,8) % D (gauss), Site 2
    % c(1,9) % E (gauss), Site 2
    % c(1,10) % Percent, Site 2
    % c(1,11) % D (gauss), Site 3
    % c(1,12) % E (gauss), Site 3
    % c(1,13) % Percent, Site 3
    % c(1,14) % D (gauss), Site 4
    % c(1,15) % E (gauss), Site 4
    % c(1,16) % Percent, Site 4
    c(1,17)=0; % t/T1x, Site 1
    c(1,18)=0; % t/T1y, Site 1
    c(1,19)=0; % t/T1z, Site 1
    % c(1,20) % t/T1x, Site 2
    % c(1,21) % t/T1y, Site 2
    % c(1,22) % t/T1z, Site 2
    % c(1,23) % t/T1x, Site 3
    % c(1,24) % t/T1y, Site 3
    % c(1,25) % t/T1z, Site 3
    % c(1,26) % t/T1x, Site 4
    % c(1,27) % t/T1y, Site 4
    % c(1,28) % t/T1z, Site 4
    c(1,29)=4.6; % T2x, Site 1
    c(1,30)=4.2; % T2y, Site 1
    c(1,31)=2.6; % T2z, Site 1
    % c(1,32) % T2x, Site 2
    % c(1,33) % T2y, Site 2
    % c(1,34) % T2z, Site 2
    % c(1,35) % T2x, Site 3
    % c(1,36) % T2y, Site 3
    % c(1,37) % T2z, Site 3
    % c(1,38) % T2x, Site 4
    % c(1,39) % T2y, Site 4
    % c(1,40) % T2z, Site 4
    % %c(1,41) % Kex, Site 1 - Redundant, not used here
```

```
% %c(1,42) % Xr, Site 1 - Redundant, not used here
% %c(1,43) % Yr, Site 1 - Redundant, not used here
% %c(1,44) % Zr, Site 1 - Redundant, not used here
% %c(1,45) % Xit, Site 1 - Redundant, not used here
% %c(1,46) % Yit, Site 1 - Redundant, not used here
% %c(1,47) % Zit, Site 1 - Redundant, not used here
% c(1,48) % Kex, Site 2
% c(1,49) % Xr, Site 2 - Euler angle alpha
% c(1,50) % Yr, Site 2 - Euler angle beta
% c(1,51) % Zr, Site 2 - Euler angle gamma
% c(1,52) % Xit, Site 2 - distribution around Euler angle, not used here
% c(1,53) % Yit, Site 2 - distribution around Euler angle, not used here
% c(1,54) % Zit, Site 2 - distribution around Euler angle, not used here
% c(1,55) % Kex, Site 3
% c(1,56) % Xr, Site 3
% c(1,57) % Yr, Site 3
% c(1,58) % Zr, Site 3
% c(1,59) % Xit, Site 3
% c(1,60) % Yit, Site 3
% c(1,61) % Zit, Site 3
% c(1,62) % Kex, Site 4
% c(1,63) % Xr, Site 4
% c(1,64) % Yr, Site 4
% c(1,65) % Zr, Site 4
% c(1,66) % Xit, Site 4
% c(1,67) % Yit, Site 4
% c(1,68) % Zit, Site 4
c(1,69)=0.64; % Ax, Site 1
c(1,70)=0.47; % Ay, Site 1
c(1,71)=0; % Az, Site 1
% c(1,72) % Ax, Site 2
% c(1,73) % Ay, Site 2
% c(1,74) % Az, Site 2
% c(1,75) % Ax, Site 3
% c(1,76) % Ay, Site 3
% c(1,77) % Az, Site 3
% c(1,78) % Ax, Site 4
% c(1,79) % Ay, Site 4
% c(1,80) % Az, Site 4
c(1,81)=0; % Isotropic, Nematic, Smectic
c(1,82)=2800; % Min field
c(1,83)=-100; % Min Y
c(1,84)=4000; % Max field
c(1,85)=100; % Max Y
c(1,86)=0; % Pixel movement
c(1,87)=1; % Number of Sites
% c(1,88) % K11 % exchange matrix terms (P11=K11 etc...)
% c(1,89) % K12
% c(1,90) % K13
% c(1,91) % K14
% c(1,92) % K21
% c(1,93) % K22
% c(1,94) % K23
% c(1,95) % K24
```

```
% c(1,96) % K31
% c(1,97) % K32
% c(1,98) % K33
% c(1,99) % K34
% c(1,100) % K41
% c(1,101) % K42
% c(1,102) % K43
% c(1,103) % K44
c(1,104)=1; % Use (1) or don't use (0) the exchange matrix
end;
Number_of_Sites=c(87);
i=sqrt(−1);
% Type of site gives me the Euler rotation angles between one site to the other,
% If alpha=beta=gama=0 then it means that it is the original site or that the site
% is different from the original site in D or E only.
syms W
for j=1:Number_of_Sites,
  s=['syms Htemp',num2str(j),' D',num2str(j),' E',num2str(j),' l',num2str(j),' m',num2str(j),' n',num2str(j)];
  eval(s);
  s=['Htemp',num2str(j),'=[−D',num2str(j),'/6*(1−3*n',num2str(j),' 2)+E',num2str(j),'/
  2*(l',num2str(j),' 2−m',num2str(j),' 2)+W W/1e10 W/1e10; W/1e10
  D',num2str(j),'/3*(1−3*n',num2str(j),' 2)−E',num2str(j),'*(l',num2str(j),' 2−m',num2str(j),' 2)
  W/1e10 ; W/1e10 W/1e10
  −D',num2str(j),'/6*(1−3*n',num2str(j),' 2)+E',num2str(j),'/
  2*(l',num2str(j),' 2−m',num2str(j),' 2)−W];   '];
  eval(s);
  s=['H(j,:,:)=Htemp',num2str(j)];
  eval(s)
end;
% Creating Symbolic Density Matrices
for j=1:Number_of_Sites,
  s=['syms     rou',num2str(j),'11     rou',num2str(j),'12     rou',num2str(j),'13     rou',num2str(j),'21
  rou',num2str(j),'22 rou',num2str(j),'23 rou',num2str(j),'31 rou',num2str(j),'32 rou',num2str(j),'33'];
  eval(s);
s=['rou',num2str(j),'=[rou',num2str(j),'11   rou',num2str(j),'12   rou',num2str(j),'13  ;  rou',num2str(j),'21
rou',num2str(j),'22 rou',num2str(j),'23 ; rou',num2str(j),'31 rou',num2str(j),'32 rou',num2str(j),'33]'];
  eval(s);
  end;
% Creating Omega Super Operator
i=sqrt(−1);
syms om
for j=1:Number_of_Sites,
  Htemp(:,:)=H(j,:,:);
  s=['om',num2str(j),'=−i*(Htemp*rou',num2str(j),'−rou',num2str(j),'*Htemp)'];
  eval(s);
  p=0;
  for k1=1:3,
    for k2=1:3
      p=p+1;
      p1=0;
      for k3=1:3,
        for k4=1:3,
          p1=p1+1;
          s=['rou',num2str(j),'11=0;']; eval(s);
```

```
            s=['rou',num2str(j),'12=0;']; eval(s);
            s=['rou',num2str(j),'13=0;']; eval(s);
            s=['rou',num2str(j),'21=0;']; eval(s);
            s=['rou',num2str(j),'22=0;']; eval(s);
            s=['rou',num2str(j),'23=0;']; eval(s);
            s=['rou',num2str(j),'31=0;']; eval(s);
            s=['rou',num2str(j),'32=0;']; eval(s);
            s=['rou',num2str(j),'33=0;']; eval(s);
            s=['rou',num2str(j),num2str(k3),num2str(k4),'=1;']; eval(s);
            s=['E99=om',num2str(j),'(',num2str(k1),',',num2str(k2),');']; eval(s);
            E9=eval(E99);
            s=['om((j-1)*9+p,(j-1)*9+p1)=E9;']; eval(s);
          end;
        end;
      end;
    end;
end;
om=om/(-i);
W=(c(82)+c(84))/2; % Gauss, for magnetic field
for j=1:Number_of_Sites,
  Type_of_Site(j,:)=[c(42+(j-1)*7) c(42+(j-1)*7+1) c(42+(j-1)*7+2) c(42+(j-1)*7+3)
  c(42+(j-1)*7+4) c(42+(j-1)*7+5)];
  s=['D',num2str(j),'=c(5+(j-1)*3);'];
  eval(s);
  s=['E',num2str(j),'=c(6+(j-1)*3);'];
  eval(s);
  D(j)=c(5+(j-1)*3);
  E(j)=c(6+(j-1)*3);
  N(j)=c(7+(j-1)*3)/100;
  T2x(j)=c(29+(j-1)*3);
  T2y(j)=c(29+(j-1)*3+1);
  T2z(j)=c(29+(j-1)*3+2);
  T1x(j)=c(17+(j-1)*3);
  T1y(j)=c(17+(j-1)*3+1);
  T1z(j)=c(17+(j-1)*3+2);
end;
K=zeros(Number_of_Sites,Number_of_Sites); % exchange rate matrix from site to site
if (c(104)==1),
for j=1:Number_of_Sites,
for k=1:Number_of_Sites,
      if (j~=k),
        K(j,k)=c(88+(j-1)*4+k-1);
      end;
    end;
  end;
else,
  for j=1:Number_of_Sites,
    for k=1:Number_of_Sites,
      if (j~=k),
        K(j,k)=c(41+(j-1)*7);
        if (c(41+(j-1)*7)>0),
          K(k,j)=c(41+(j-1)*7);
        end;
      end;
```

```
        end;
      end;
    end;
    for j=1:Number_of_Sites,
      Ax(j)=c(69+(j−1)*3);
      Ay(j)=c(69+(j−1)*3+1);
      Az(j)=c(69+(j−1)*3+2);
    end;
    xsix=((D+E)/2/W+1)/2;
    xsiy=((E−D)/2/W+1)/2;
    xsiz=(E/W+1)/2;
    alphat=Ax+Ay+Az;
    alphax=(1−3*Ax./alphat)/2;
    alphay=(1−3*Ay./alphat)/2;
    alphaz=(1−3*Az./alphat)/2;
    alphax1=(1−2*alphax)/3;
    alphay1=(1−2*alphay)/3;
    alphaz1=(1−2*alphaz)/3;
    for j=1:Number_of_Sites,
    alphamax(j)=max([alphax1(j) alphay1(j) alphaz1(j)]);
    end;
    alphax1=alphax1./alphamax;
    alphay1=alphay1./alphamax;
    alphaz1=alphaz1./alphamax;
    alphat=alphax1+alphay1+alphaz1;
    betax=(1−2*xsix).*(alphay1−alphaz1)./alphat;
    betay=(1−2*xsiy).*(alphaz1−alphax1)./alphat;
    betaz=(1−2*xsiz).*(alphax1−alphay1)./alphat;
    Thermal_Pop=0.0001;
    Tx1=(−alphax+betax).*exp(−3*T1x)+Thermal_Pop*(1−exp(−3*T1x));
    Tx2=(alphax+betax).*exp(−3*T1x)+Thermal_Pop*(1−exp(−3*T1x));
    Ty1=(−alphay+betay).*exp(−3*T1y)+Thermal_Pop*(1−exp(−3*T1y));
    Ty2=(alphay+betay).*exp(−3*T1y)+Thermal_Pop*(1−exp(−3*T1y));
    Tz1=(−alphaz+betaz/2).*exp(−3*T1z)+Thermal_Pop*(1−exp(−3*T1z));
    Tz2=(alphaz+betaz/2).*exp(−3*T1z)+Thermal_Pop*(1−exp(−3*T1z));
    In=zeros(Np,1);
    % super-matrix of exchange between sites
    KS=zeros(Number_of_Sites*9,Number_of_Sites*9);
    for j=1:Number_of_Sites,
      for j1=1:Number_of_Sites,
        for k=1:9,
          if (j==j1),
            KS((j−1)*9+k,(j1−1)*9+k)=−sum(K(:,j));
          else,
            KS((j−1)*9+k,(j1−1)*9+k)=(K(j,j1));
          end;
        end;
      end;
    end;
    KS=−KS;
    % SX super vector
    Jx=1/sqrt(2)*[0 1 0 ;1 0 1; 0 1 0]; % Jx in 1 ,0, −1 basis
    Jy=1/sqrt(2)*[0 −i 0 ;i 0 −i; 0 i 0]; % Jy in 1,0 , −1 basis
    Jz=[1 0 0 ;0 0 0; 0 0 −1]; % Jz in 1,0 ,−1 basis
```

```
Sx=[0 0 0 ; 0 0 −i ; 0 i 0];
Sx=Jx;
Sp=Jx+sqrt(−1)*Jy;
% isotropic case
if (c(81)==0),
  h9 = waitbar(0,'Please wait. . .');
  for Theta=0.001:0.02:pi/2, % Loop on Theta. This is the numerical integration parameter
    waitbar(Theta/1.57,h9);
    for Phi=0.001:0.02:pi/2, % Loop on Phi. This is the numerical integration parameter
      % Hamiltonian for Z axis facing molecule, Z∥B0
      %Creating The Sites Hamiltonian
      l1=(sin(Theta)*cos(Phi));
      m1=(sin(Theta)*sin(Phi));
      n1=(cos(Theta));
      TT11=eval('Tx1(1)*l1 2+Ty1(1)*m1 2+Tz1(1)*n1 2');
      TT12=eval('Tx2(1)*l1 2+Ty2(1)*m1 2+Tz2(1)*n1 2');
      for j=2:Number_of_Sites,
        % Euler Rotation
        Reuler=euler(Type_of_Site(j,1),Type_of_Site(j,2),Type_of_Site(j,3));
        s=['atemp=Reuler*[l1 ; m1 ; n1];'];
        eval(s);
        s=['l',num2str(j),'=atemp(1); m',num2str(j),'=atemp(2); n',num2str(j),'=atemp(3);'];
        eval(s);
        s=['TT',num2str(j),'1=eval("Tx1(',num2str(j),')*l',num2str(j),' 2+Ty1(',num2str(j),')*m',num2str(j),'
        2+Tz1(',num2str(j),')*n',num2str(j),' 2");'];
        eval(s);
        s=['TT',num2str(j),'2=eval("Tx2(',num2str(j),')*l',num2str(j),' 2+Ty2(',num2str(j),')*m',num2str(j),'
        2+Tz2(',num2str(j),')*n',num2str(j),' 2");'];
        eval(s)
      end;
      % T2 Relaxation Super Operator
      ind_mat=eye(Number_of_Sites*9);
      T2_mat=zeros(Number_of_Sites*9,Number_of_Sites*9);
      for j=1:Number_of_Sites,
        s=['T2_real=l',num2str(j),' 2*T2x(j)+m',num2str(j),' 2*T2y(j)+n',num2str(j),' 2*T2z(j);'];
        eval(s);
        T2_mat((j−1)*9+2,(j−1)*9+2)=T2_real;
        T2_mat((j−1)*9+3,(j−1)*9+3)=T2_real;
        T2_mat((j−1)*9+4,(j−1)*9+4)=T2_real;
        T2_mat((j−1)*9+6,(j−1)*9+6)=T2_real;
        T2_mat((j−1)*9+7,(j−1)*9+7)=T2_real;
          T2_mat((j−1)*9+8,(j−1)*9+8)=T2_real;
      end;
      SX=zeros(Number_of_Sites*9,1);
      for j=1:Number_of_Sites,
        pp=0;
        for j1=1:3,
          for j2=1:3,
            pp=pp+1;
            SX((j−1)*9+pp,1)=Sp(j1,j2);
          end;
        end;
      end;
      % Creating Omega Super Operator
```

```
om99=eval(om);
% Semi - Equilibrium rou
rou0=zeros(Number_of_Sites*9,Number_of_Sites*9);
for j=1:Number_of_Sites,
   kq=0;
   for j1=1:3,
      for j2=1:3,
         kq=kq+1;
         s=['rou0((j−1)*9+2,(j−1)*9+2)=TT',num2str(j),'2*N(',num2str(j),');'];
         eval(s)
         s=['rou0((j−1)*9+6,(j−1)*9+6)=TT',num2str(j),'1*N(',num2str(j),');'];
         eval(s)
      end;
   end;
end;
% distribution function calculation for isotropic case
dist_funct=sin(Theta);
pq=0;
for FW=c(82):(c(84)−c(82))/(Np−1):c(84); % Gauss, for changing frequency of microwave irradiation
   pq=pq+1;
   Q=(om99−FW*ind_mat)−i*(KS+T2_mat);
   In(pq)=In(pq)+dist_funct*(2*imag(trace(rou0*SX*(Q (−1)*SX).')));
end;
   end;
   end;
   close(h9);
end;
XXX=c(82):(c(84)−c(82))/(Np−1):c(84);
YYY=In;
```

REFERENCES

1. Weil JA, Bolton JR, Wertz JE. 1994. Electron paramagnetic resonance. New York: Wiley.

2. Carrington A, McLachlan AD. 1967. Introduction to magnetic resonance with applications to chemistry and chemical physics. New York: Harper & Row.

3. Stavitski E, Berg A, Ganguly T, Mahammed A, Gross Z, Levanon H. 2004. Electron spin dynamics in photo-excited diamagnetic and paramagnetic corroles. J Am Chem Soc 126:6886–6890.

4. Gonen O, Levanon H. 1984. Line shape analysis of transient triplet electron paramagnetic resonance spectra. Application to porphyrins and chlorophylls in nematic uniaxial liquid crystals. J Phys Chem 88:4223–4228.

5. Shain AL. 1972. Dynamics of intramolecular triplet exciton transfer using electron-spin resonance. J Chem Phys 56:6201–6212.

6. Levanon H, Vega S. 1974. Analysis of transient EPR signals in photoexcited triplet state-application to porphyrin molecules. J Chem Phys 61:2265–2274.

7. Norris JR, Weissman SI. 1969. Studies of rotational diffusion through electron-electron dipolar interaction. J Phys Chem 73:3119–3124.

8. de Groot MS, van der Waals JH. 1963. Paramagnetic resonance in phosphorescent hydrocarbons. III. Conformational isomerism in benzene and triptycene. Mol Phys 6:545–562.

9. Bramwell FB, Gendell J. 1970. ESR Studies of phosphorescent corannulene. Evidence for pseudorotation. J Chem Phys 52:5656–5661.

10. Haarer D, Wolf HC. 1970. ESR Studies on triplet excitons in anthracene and naphthalene monocrystals. Mol Cryst Liq Cryst 10:359–380.

11. Murai H, Yamauchi S, Kawai A, Obi K, Hirota N. 2003. Developments of magnetic resonance-related spin chemistry in Japan. Appl Magn Reson 23:249–267.

12. Freed JH, Bruno GV, Polnasze C. 1971. ESR line shapes for triplets undergoing slow rotational reorientation. J Chem Phys 55:5270–5281.

13. Gamliel D, Levanon H. 1992. Electron paramagnetic resonance line shapes of photoexcited triplets with rotational diffusion. J Chem Phys 97:7140–7159.

14. Regev A, Galili T, Levanon H. 1991. The photoexcited triplet state as a probe of dynamics and phase memory in a multiphase liquid crystal: time-resolved electron

paramagnetic resonance spectroscopy. J Chem Phys 95:7907–7916.

15. Alexander S. 1962. Exchange of interacting nuclear spins in nuclear magnetic resonance. 1. Intramolecular exchange. J Chem Phys 37:967–973.

16. Atherton NM. 1992. Principles of electron spin resonance. Chichester: Ellis Horwood.

17. Gamliel D, Freed JH. 1990. Theory of 2-dimensional ESR with nuclear modulation. J Magn Reson 89:60–93.

18. Hutchison C, Mangum BW. 1961. Paramagnetic resonance absorption in naphthalene in its phosphorescent state. J Chem Phys 34:908–922.

19. Abragam A. 1961. The principles of nuclear magnetism. Oxford: Clarendon Press p 101.

20. Hudson A, McLachlan AD. 1965. Line shapes of triplet ESR spectra-effects of intermolecular exciton transfer. J Chem Phys 43:1518–1524.

21. Sakurai JJ, Tuan SF. 1994. Modern quantum mechanics. Reading, MA: Addison-Wesley pp 83–84.

22. Kubo R. 1969. Stochastic theories of randomly modulated systems. J Phys Soc Jpn 26(Suppl):1–6.

23. Gamliel D, Levanon H. 1995. Stochastic processes in magnetic resonance. Singapore: World Scientific.

24. Wong SK, Hutchins DA, Wan JKS. 1973. Chemically induced dynamic electron polarization. 2. General theory for radicals produced by photochemical reactions of excited triplet carbonyl-compounds. J Chem Phys 58:985–989.

25. Redfield AG. 1957. On the theory of relaxation processes. IBM J Res Dev 1:19–31.

26. Kubo R, Tomita K. 1954. A general theory of magnetic resonance absorption. J Phys Soc Jpn 9:888–919.

27. Alexander S. 1962. Exchange of interacting nuclear spins in nuclear magnetic resonance. 2. Chemical exchange. J Chem Phys 37:974–980.

28. Wasserman E, Yager WA, Snyder LC. 1964. ESR of triplet states of randomly oriented molecules. J Chem Phys 41:1763–1772.

29. Hiromitsu I, Kevan L. 1988. An improved analysis of transient electron-spin-resonance signals of photoexcited triplet states—application to chlorophyll a in a glassy matrix. J Chem Phys 88:691–695.

30. Pake GE. 1948. Nuclear resonance absorption in hydrated crystals: fine structure of the proton line. J Chem Phys 16:327–336.

31. Berman A, Levanon H, Vogel E, Jux N. 1993. Triplet spin alignment of stretched porphycenes. Chem Phys Lett 211:549–554.

32. Stegemeyer H. 1994. Liquid crystals. Darmstadt and New York: Steinkopff; Springer.

33. Regev A, Gamliel D, Meiklyar V, Michaeli S, Levanon H. 1993. Dynamics of $^{3}C_{60}$ probed by electron paramagnetic resonance-motional analysis in isotropic and liquid crystalline matrices. J Phys Chem 97:3671–3679.

34. Stillman AE, Zientara GP, Freed JH. 1979. The variational method and the stochastic Liouville equation. II. ESR spectral simulation via finite elements. J Chem Phys 71:113–118.

35. Yamauchi S, Takahashi A, Iwasaki Y, Unno M, Ohba Y, Higuchi J, Blank A, Levanon H. 2003. The lowest photoexcited triplet state of subphthalocyanine in solid and fluid environments. Time-resolved electron paramagnetic resonance studies. J Phys Chem A 107:1478–1485.

36. Yamauchi S. 2004. Recent developments in studies of electronic excited states by means of electron paramagnetic resonance spectroscopy. Bull Chem Soc Jpn 77:1255–1268.

BIOGRAPHIES

Aharon Blank was born in Haifa, Israel. He received his Ph.D. degree from the Hebrew University of Jerusalem (2002) in physical chemistry. He is currently working on his postdoctoral research with Prof. J. Freed at Cornell University and holds a senior lecturer position in the faculty of chemistry at the Technion–Israel Institute of Technology. His research interests include ESR and NMR spectroscopy (theory and experimental methods), chemically induced dynamic electron spin polarization (theoretical and experimental aspects), electromagnetic waves propagation and scattering, signal processing techniques, magnetic resonance imaging, and the applications of magnetic resonance in general.

Haim Levanon was born in Jerusalem, Israel. He received his Ph.D. degree from the Hebrew University of Jerusalem (1969) in physical chemistry. After his postdoctoral research with Prof. S. Weissman at Washington University, he joined the department of physical chemistry at the Hebrew University of Jerusalem, where he is currently a full professor. His research interests are in the field of time-resolved EPR, model photosynthesis, electron transfer and liquid crystals, photophysics and photochemistry of fullerenes, polarized electrons in photoexcited solutions of alkali metals, and microwave devices based on electron spin polarization at room temperature. Prof. Levanon was awarded the Max Planck research award (1992) and the Alexander von Humboldt award (2002). He is currently serving as editor-in-chief of the *Israel Journal of Chemistry.*